

$B\bar{B}$ angular correlations at the LHC in the parton Reggeization approach merged with higher-order matrix elementsA. V. Karpishkov,^{*} M. A. Nefedov,[†] and V. A. Saleev[‡]*Samara National Research University, Moscow Highway, 34, 443086 Samara, Russia*

(Received 14 July 2017; published 21 November 2017)

We calculate the angular distribution spectra between beauty (B) and antibeauty (\bar{B}) mesons in proton-proton collisions in the leading order approximation of the parton Reggeization approach consistently merged with the next-to-leading order corrections from the emission of an additional hard gluon. To describe b -quark hadronization we use the universal scale-dependent parton-to-meson fragmentation functions extracted from the world e^+e^- annihilation data. We have obtained good agreement between our predictions and data from the CMS Collaboration at the energy $\sqrt{S} = 7$ TeV for $B\bar{B}$ angular correlations within uncertainties and without free parameters. Predictions for analogous correlation observables at $\sqrt{S} = 13$ TeV are provided.

DOI: [10.1103/PhysRevD.96.096019](https://doi.org/10.1103/PhysRevD.96.096019)**I. INTRODUCTION**

Production of b -quarks in the high energy pp -collisions is the object of an intensive experimental study at the CERN LHC. In the present paper we focus on measurements of $b\bar{b}$ angular and momentum correlations, since they provide a test of dynamics of hard interactions, which is highly sensitive to the higher-order corrections in QCD. There are two ways of studying these $b\bar{b}$ correlations. The first one is based on reconstruction of pairs of b -jets [1,2]; in the second case we get information on dynamics of the hard production of $b\bar{b}$ -pairs using data on pair production of B -mesons. In turn, long-lived B -mesons are reconstructed via their semileptonic decays. One advantage of the latter method is the unique capability to detect $B\bar{B}$ -pairs even at small opening angles, in which case the decay products of the B -hadrons tend to be merged into a single jet and the standard b -jet tagging techniques are not applicable [3].

On the theory side, apart from multiple radiation of soft/collinear additional partons one has to take into account radiation of hard additional partons to describe such angular correlations over the whole observable range of opening angles between momenta of B -mesons. In the leading order (LO) of the collinear parton model (CPM), b -quarks are produced back to back at an azimuthal angle. Effects of the soft and collinear Initial State Radiation (ISR) or Final State Radiation (FSR) somewhat smear the distribution in the azimuthal angle difference between transverse momenta of mesons ($\Delta\phi$) around $\Delta\phi \approx \pi$. These effects are systematically taken into account with the Leading Logarithmic Accuracy in the Parton Showers

(PS) of the standard Monte Carlo (MC) generators, such as PYTHIA or HERWIG.

Radiation of the additional hard gluons or quarks causes B and \bar{B} mesons to fly with $\Delta\phi < \pi$, but such radiation is beyond the formal accuracy of standard PS. Description of such events essentially depends on the way that transverse momentum and the “small” light-cone component of the momentum of the emitted parton are dealt with inside a PS algorithm, the so-called “recoiling scheme” [4]. Usually the accuracy of the description of such kinematic configurations is improved via different methods of *matching* the full NLO corrections in the CPM with the parton shower, such as MC@NLO [5] or POWHEG [6], or via *merging* of the kinematically and dynamically accurate descriptions of a few additional hard emissions, provided by the exact tree-level matrix elements, with the soft/collinear emissions from the PS [7,8].

The presence of additional free parameters in the matching/merging methods, as well as the multitude of possible recoiling schemes, clearly calls for the improved understanding of the high- p_T regime of the PS from the point of view of Quantum Field Theory. Apart from the soft and collinear limits, the only known limit of scattering amplitudes in QCD whose structure is sufficiently simple for the theoretical analysis is the limit of multi-Regge kinematics (MRK), when emitted partons are highly separated in rapidity from each other. This makes the MRK limit a natural starting point for the construction of improved approximations. In the present paper, we construct the factorization formula and the framework of LO calculations in the parton Reggeization approach (PRA), which unifies the PS-like description of the soft and collinear emissions with the MRK limit for hard emissions. Then we switch to the description of the angular correlations in the production of $B\bar{B}$ -pairs accompanied by the hard jet, which sets the scale of the process. The present

^{*}karpishkov@rambler.ru[†]nefedovma@gmail.com[‡]saleev@samsu.ru

study is motivated by the experimental data of Ref. [3]. In Ref. [3] the predictions of PYTHIA6.4 MC event generator [9], MC@NLO predictions [5] matched to the HERWIG6.5 MC event generator [10], and the predictions in the MadGraph + MadEvent framework [11,12] were compared to the experimental data. Neither the above-mentioned MC calculations in the framework of collinear factorization nor the calculations employing the CASCADE MC event generator [13], based on the Ciafaloni-Catani-Fiorani-Marchesini evolution equation [14] or the LO of k_T -factorization approach in Ref. [15], could accurately describe the shape of angular distributions. A very similar situation has been found in a recent measurement of $B\bar{B}$ -correlations, performed by the ATLAS Collaboration [16] in the pp -collisions at $\sqrt{S} = 8$ TeV. Comparison of the experimental data with different options of PYTHIA8.1 [17] and SHERPA [18] MC event generators in Figs. 7, 8, and 9 of Ref. [16] is especially interesting. These figures show the large spread between predictions of different event generators or different options of the same event generator, which amounts up to $\pm 50\%$ in some bins.

In the present paper, we construct the consistent prescription, which merges the LO PRA calculation for this process with tree-level NLO matrix element. The latter improves the description of those events, in which not the b -jet, but the hard gluon jet is the leading one, while avoiding possible double-counting and divergence problems. In such a way we achieve a good description of the shape of all $B\bar{B}$ correlation spectra without additional free parameters.

The paper has the following structure. We describe the basics of the PRA and its relationships to other approaches in Sec. II. In Sec. III we present our merging prescription and the analytic and numerical tools that we use. Then we concentrate on the numerical results, comparison with experimental data of Ref. [3], and predictions for possible future measurements in Sec. IV. Finally, we summarize our conclusions in Sec. V.

II. LO PRA FRAMEWORK

To derive the factorization formula of the PRA in the LO approximation, let us consider production of the partonic final state of interest \mathcal{Y} in the following auxiliary hard subprocess:

$$g(p_1) + g(p_2) \rightarrow g(k_1) + \mathcal{Y}(P_A) + g(k_2), \quad (1)$$

where the four-momenta of particles are denoted in parentheses, and $p_1^2 = p_2^2 = k_1^2 = k_2^2 = 0$. The final state \mathcal{Y} sets the hard scale μ^2 of the whole process via its invariant mass $M_A^2 = P_A^2$, or transverse momentum $P_{T,A}$; otherwise it can be an arbitrary combination of QCD partons. In a frame where $\mathbf{p}_1 = -\mathbf{p}_2$ is directed along

the Z-axis, it is natural to work with the Sudakov (light-cone) components of any four-momentum k :

$$k^\mu = \frac{1}{2}(k^+ n_\pm^\mu + k^- n_\mp^\mu) + k_T^\mu,$$

where $n_\pm^\mu = (n^\pm)^\mu = (1, 0, 0, \mp 1)^\mu$; $n_\pm^2 = 0$; $n_+ n_- = 2$; $k^\pm = k_\pm = (n_\pm k) = k^0 \pm k^3$; and $n_\pm k_T = 0$, so that $p_1^- = p_2^+ = 0$ and $s = (p_1 + p_2)^2 = p_1^+ p_2^- > 0$. The dot product of two four-vectors k and q in this notation is equal to

$$(kq) = \frac{1}{2}(k^+ q_- + k^- q_+) - \mathbf{k}_T \mathbf{q}_T.$$

For the discussion of different kinematic limits of the process (1) it is convenient to introduce the “ t -channel” momentum transfers $q_{1,2} = p_{1,2} - k_{1,2}$, which implies that $\mathbf{q}_{T,1,2} = -\mathbf{k}_{T,1,2}$, $q_1^- = -k_1^-$, and $q_2^+ = -k_2^+$. Let us define $t_{1,2} = \mathbf{q}_{T,1,2}^2$, and the corresponding fractions of the “large” light-cone components of momenta,

$$z_1 = \frac{q_1^+}{p_1^+}, \quad z_2 = \frac{q_2^-}{p_2^-},$$

for the further use. The variables $z_{1,2}$ satisfy the conditions $0 \leq z_{1,2} \leq 1$ because $k_{1,2}^\pm \geq 0$ and $q_1^+ = P_A^+ + k_2^+ \geq 0$, $q_2^- = P_A^- + k_1^- \geq 0$ since all final-state particles are on shell.

In the *collinear limit* (CL), when $\mathbf{k}_{T,1,2}^2 \ll \mu^2$, while $0 \leq z_{1,2} \leq 1$, the asymptotic for the square of the tree-level matrix element for the subprocess (1) is very well known:

$$\overline{|\mathcal{M}|^2}_{\text{CL}} \simeq \frac{4g_s^4}{\mathbf{k}_{T1}^2 \mathbf{k}_{T2}^2} P_{gg}(z_1) P_{gg}(z_2) \frac{|\overline{\mathcal{A}_{\text{CPM}}}|^2}{z_1 z_2}, \quad (2)$$

where the bar denotes averaging (summation) over the spin and color quantum numbers of the initial-state (final-state) partons, $g_s = \sqrt{4\pi\alpha_s}$ is the coupling constant of QCD, $P_{gg}(z) = 2C_A((1-z)/z + z/(1-z) + z(1-z))$ is the LO gluon-gluon Dokshitzer-Gribov-Lipatov-Altarelli-Parisi (DGLAP) splitting function, and \mathcal{A}_{CPM} is the amplitude of the subprocess $g(z_1 p_1) + g(z_2 p_2) \rightarrow \mathcal{Y}(P_A)$ with on-shell initial-state gluons. The error of approximation (2) is suppressed as $O(\mathbf{k}_{T,1,2}^2/\mu^2)$ with respect to the leading term.

The limit of MRK for the subprocess (1) is defined as

$$\Delta y_1 = y(k_1) - y(P_A) \gg 1, \quad \Delta y_2 = y(P_A) - y(k_2) \gg 1, \quad (3)$$

$$\mathbf{k}_{T1}^2 \sim \mathbf{k}_{T2}^2 \sim M_{T,A}^2 \sim \mu^2 \ll s, \quad (4)$$

where rapidity for the four-momentum k is equal to $y(k) = \frac{1}{2} \log(\frac{k^+}{k^-})$. The rapidity gaps $\Delta y_{1,2}$ can be calculated as

$$\Delta y_{1,2} = \log \left[\frac{M_{TA}}{|\mathbf{k}_{T1,2}|} \frac{1 - z_{1,2}}{z_{1,2} - \frac{\mathbf{k}_{T2,1}^2}{s(1-z_{2,1})}} \right].$$

From this expression, taken together with the conditions (3) and (4), one can see that the following hierarchy holds in the MRK limit,

$$\frac{\mathbf{k}_{T1,2}^2}{s} \ll z_1 \sim z_2 \ll 1, \quad (5)$$

so that the small parameters, which control the MRK limit, are actually $z_{1,2}$, while the transverse momenta are of the same order of magnitude as the hard scale, and the collinear asymptotic of the amplitude (2) is inapplicable. Also, the following scaling relations for momentum components hold in the MRK limit:

$$\begin{aligned} M_{TA} &\sim |\mathbf{k}_{T1}| \sim q_1^+ \sim O(z_1) \gg q_1^- \sim O(z_1^2), \\ M_{TA} &\sim |\mathbf{k}_{T2}| \sim q_2^- \sim O(z_2) \gg q_2^+ \sim O(z_2^2), \end{aligned} \quad (6)$$

which allows one to neglect the ‘‘small’’ light-cone components of momenta q_1^- and q_2^+ .

The systematic formalism for the calculation of the asymptotic expressions for arbitrary QCD amplitudes in the MRK limit has been formulated by Lipatov and Vyazovsky in a form of gauge-invariant Effective Field Theory (EFT) for multi-Regge processes in QCD [19,20], see also [21] for a review. The MRK asymptotics of the amplitude in this EFT is constructed from gauge-invariant blocks—*effective vertices*, which describe the production of clusters of QCD partons, separated by the large rapidity gaps. These effective vertices are connected together via t -channel exchanges of gauge-invariant off-shell degrees of freedom, Reggeized gluons R_\pm , and Reggeized quarks Q_\pm . The latter obey special kinematical constraints, such that the field $Q_\pm(R_\pm)$ carries only the q^\pm light-cone component of momentum and the transverse momentum of the same order of magnitude, while $q^\mp = 0$. As shown above, these kinematical constraints are equivalent to MRK.

Due to the requirements of gauge invariance of the effective vertices and the above-mentioned kinematic constraints, the interactions of QCD partons and Reggeons in the EFT [19,20] are nonlocal and contain the Wilson’s exponents of gluonic fields. After the perturbative expansion, the latter generate an infinite series of induced vertices of interaction of particles and Reggeons. The Feynman rules of the EFT are worked out in detail in Ref. [22]; however, we also collect the induced and effective vertices, relevant for our present study, in Figs. 1 and 2 for the reader’s convenience.

The diagrammatic representation of the squared amplitude of the process (1) is shown in Fig. 3. Explicitly, the $R_\pm gg$ effective vertex, which is depicted diagrammatically in Fig. 2, reads

$$\begin{aligned} \Gamma_{\mu\nu\pm}^{abc}(k_1, k_2) &= -ig_s f^{abc} \left[2g_{\mu\nu} k_1^\mp + (2k_2 + k_1)_\mu n_\nu^\mp \right. \\ &\quad \left. - (2k_1 + k_2)_\nu n_\mu^\mp - \frac{(k_1 + k_2)^2}{k_1^\mp} n_\mu^\mp n_\nu^\mp \right]. \end{aligned}$$

By evaluating the square of $R_\pm gg$ effective vertex, contracted with the polarization vectors of on-shell external gluons, one obtains

$$\sum_{\lambda_1, \lambda_2} |\Gamma_{\mu\nu\pm}(k_1, -k_2) \epsilon_\mu(k_1, \lambda_1) \epsilon_\nu^*(k_2, \lambda_2)|^2 = 8(k_1^\mp)^2. \quad (7)$$

Using the result (7) and the Feynman rules of Fig. 1, one can write the MRK asymptotics of the squared amplitude of the process (1) in the following form,

$$|\overline{\mathcal{M}}|^2_{\text{MRK}} \simeq \frac{4g_s^4}{\mathbf{k}_{T1}^2 \mathbf{k}_{T2}^2} \tilde{P}_{gg}(z_1) \tilde{P}_{gg}(z_2) \frac{|\overline{\mathcal{A}}_{\text{PRA}}|^2}{z_1 z_2}, \quad (8)$$

where the MRK gluon-gluon splitting functions $\tilde{P}_{gg}(z) = 2C_A/z$ reproduce the small- z asymptotics of the full DGLAP splitting functions and the squared PRA amplitude is defined as

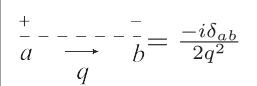
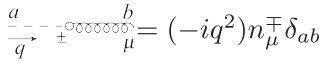
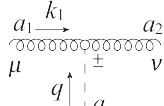
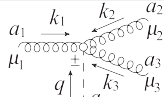
	
	$g_s f_{a a_1 a_2} (n_\mu^\mp n_\nu^\mp) \frac{q^2}{k_1^\mp}$
	$ig_s^2 (n_{\mu_1}^\mp n_{\mu_2}^\mp n_{\mu_3}^\mp) \frac{q^2}{k_3^\mp} \left[\frac{f_{a b a_1} f_{b a_2 a_3}}{k_1^\mp} + \frac{f_{a b a_2} f_{b a_1 a_3}}{k_2^\mp} \right]$

FIG. 1. Feynman rules of the EFT [19]. The propagator of the Reggeized gluon (top left panel) and Reggeon-gluon induced vertices up to the $O(g_s^2)$ are shown. The usual Feynman rules of QCD hold for interactions of ordinary quarks and gluons.

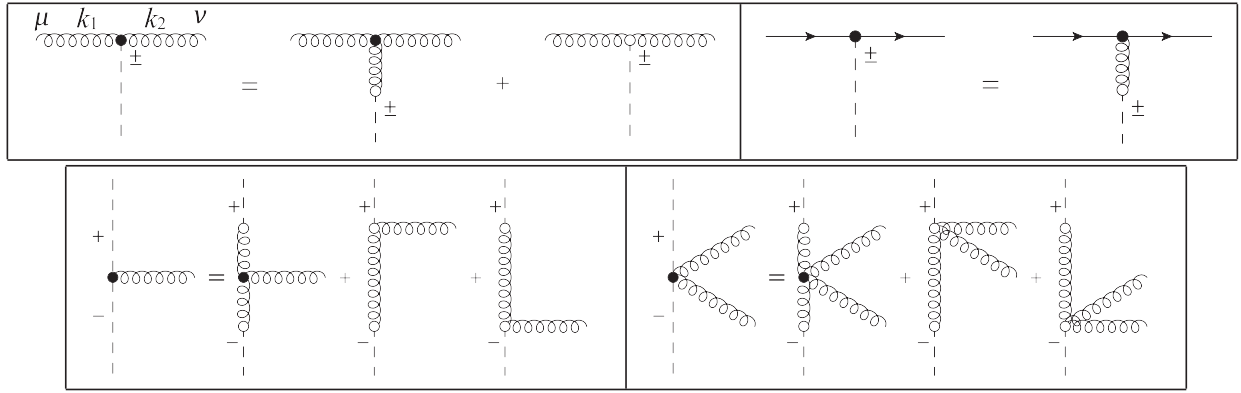


FIG. 2. Structure of the effective vertices $R_{\pm}gg$ (top left), $R_{\pm}q\bar{q}$ (top right), $R_{+}R_{-}g$ (bottom left), and the $R_{+}R_{-}gg$ combined vertex (bottom right). These vertices appear in the diagrams of Figs. 3, 5, and 7.

$$\overline{|\mathcal{A}_{\text{PRA}}|^2} = \left(\frac{q_1^+ q_2^-}{4(N_c^2 - 1)\sqrt{t_1 t_2}} \right)^2 [\mathcal{A}_{c_1 c_2}^* \mathcal{A}^{c_1 c_2}], \quad (9)$$

where \mathcal{A} is the Green's function of the subprocess $R_{+}(q_1) + R_{-}(q_2) \rightarrow \mathcal{Y}(\mathcal{P}_{\mathcal{A}})$ with amputated propagators of the Reggeized gluons, and $c_{1,2}$ are their color indices. The error of the approximation (8) is suppressed as $O(z_{1,2})$ with respect to the leading term.

In contrast with the collinear limit, the PRA amplitude explicitly and nontrivially depends on the \mathbf{q}_{T1} and \mathbf{q}_{T2} . However, when $\mathbf{k}_{T1,2} \ll \mu^2$, the MRK limit reduces to the small- $z_{1,2}$ asymptotics of the collinear limit and Eq. (8) should reproduce Eq. (2). To this end, the following *collinear limit constraint* for the PRA amplitude should hold:

$$\int \frac{d\phi_1 d\phi_2}{(2\pi)^2} \lim_{t_{1,2} \rightarrow 0} \overline{|\mathcal{A}_{\text{PRA}}|^2} = \overline{|\mathcal{A}_{\text{CPM}}|^2}, \quad (10)$$

where $\phi_{1,2}$ are the azimuthal angles of the vectors $\mathbf{q}_{T1,2}$. One can prove the constraint (10) for the general PRA amplitudes

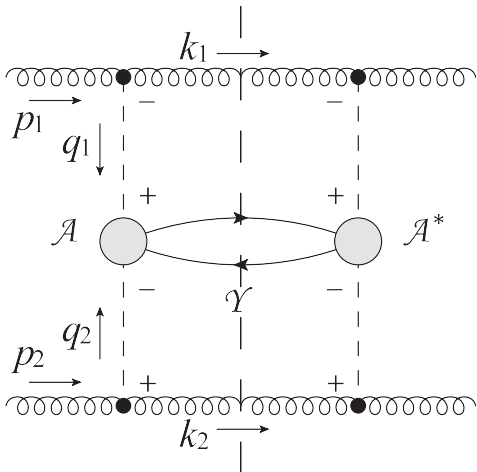


FIG. 3. Diagrammatic representation of the MRK asymptotics for the squared amplitude of the subprocess (1).

of the type $R_{+} + R_{-} \rightarrow \mathcal{Y}$, with the help of Ward identities for the Green's functions with Reggeized gluons, which has been discovered in Ref. [23].

Now we introduce the *modified MRK (mMRK) approximation* for the squared amplitude of the subprocess (1) as follows:

- (1) In Eq. (8) we substitute the MRK asymptotics for the splitting functions $\tilde{P}_{gg}(z)$ by the full LO DGLAP expression $P_{gg}(z)$.
- (2) We substitute the factors $\mathbf{k}_{T1,2}^2$ in the denominator of (8) by the exact value of $q_{1,2}^2$, as if all four components of momentum $q_{1,2}^+$, $q_{1,2}^-$, and \mathbf{q}_T were flowing through the t -channel propagator: $\mathbf{k}_{T1,2}^2 \rightarrow -q_{1,2}^2 = \mathbf{q}_{T1,2}^2/(1 - z_{1,2})$.
- (3) However, the “small” light-cone components of momenta, q_1^- and q_2^+ , do not propagate into the hard scattering process, so its gauge-invariant definition is unaffected and is given by Lipatov's EFT [19].

After these substitutions, the mMRK approximation for the squared amplitude of the subprocess (1) takes the following form:

$$\overline{|\mathcal{M}|^2}_{\text{mMRK}} \simeq \frac{4g_s^4}{q_1^2 q_2^2} P_{gg}(z_1) P_{gg}(z_2) \frac{\overline{|\mathcal{A}_{\text{PRA}}|^2}}{z_1 z_2}. \quad (11)$$

The mMRK approximation (11) reproduces the exact QCD results both in the collinear and MRK limits. The latter suggests that it should be more accurate than the default collinear limit approximation (2) when $\mathbf{k}_{T1,2} \sim \mu^2$ even outside of the strict MRK limit $z_{1,2} \ll 1$; however, at present we cannot give the precise parametric estimate of accuracy of Eq. (11) in this kinematic region. The available numerical evidence (see Ref. [24] for the case of amplitudes with Reggeized gluons in the t -channel and Refs. [25,26] for the case of Reggeized quarks) supports the form of mMRK approximation proposed above.

To derive the LO factorization formula of the PRA we substitute the mMRK approximation (11) into the factorization formula of the CPM integrated over the phase space of additional partons $k_{1,2}$:

$$\begin{aligned} d\sigma &= \int \frac{dk_1^+ d^2\mathbf{k}_{T1}}{(2\pi)^3 k_1^+} \int \frac{dk_2^- d^2\mathbf{k}_{T2}}{(2\pi)^3 k_2^-} \int d\tilde{x}_1 d\tilde{x}_2 f_g(\tilde{x}_1, \mu^2) \\ &\times f_g(\tilde{x}_2, \mu^2) \frac{|\overline{\mathcal{M}}|_{\text{mMRK}}^2}{2S\tilde{x}_1\tilde{x}_2} (2\pi)^4 \\ &\times \delta\left(\frac{1}{2}(q_1^+ n_- + q_2^- n_+) + q_{T1} + q_{T2} - P_A\right) d\Phi_A, \end{aligned} \quad (12)$$

where $f_g(x, \mu^2)$ are the (integrated) Parton Distribution Functions (PDFs) of the CPM, $p_{1,2}^\mu = \tilde{x}_{1,2} P_{1,2}^\mu$, where $P_{1,2}$ are the four-momenta of colliding protons, and $d\Phi_A$ is the element of the Lorentz-invariant phase space for the final state of the hard subprocess \mathcal{Y} .

Changing the variables in the integral, $(k_1^+, \tilde{x}_1) \rightarrow (z_1, x_1)$, $(k_2^-, \tilde{x}_2) \rightarrow (z_2, x_2)$, where $x_{1,2} = \tilde{x}_{1,2} z_{1,2}$, one can rewrite Eq. (12) in a k_T -factorized form:

$$\begin{aligned} d\sigma &= \int_0^1 \frac{dx_1}{x_1} \int \frac{d^2\mathbf{q}_{T1}}{\pi} \tilde{\Phi}_g(x_1, t_1, \mu^2) \\ &\times \int_0^1 \frac{dx_2}{x_2} \int \frac{d^2\mathbf{q}_{T2}}{\pi} \tilde{\Phi}_g(x_2, t_2, \mu^2) \cdot d\hat{\sigma}_{\text{PRA}}, \end{aligned} \quad (13)$$

where the partonic cross section in the PRA is given by

$$\begin{aligned} d\hat{\sigma}_{\text{PRA}} &= \frac{|\overline{\mathcal{A}}_{\text{PRA}}|^2}{2Sx_1x_2} \cdot (2\pi)^4 \delta\left(\frac{1}{2}(q_1^+ n_- + q_2^- n_+) \right. \\ &\left. + q_{T1} + q_{T2} - P_A\right) d\Phi_A, \end{aligned} \quad (14)$$

and the tree-level ‘‘unintegrated PDFs’’ (unPDFs) are

$$\tilde{\Phi}_g(x, t, \mu^2) = \frac{1}{t} \frac{\alpha_s}{2\pi} \int_x^1 dz P_{gg}(z) \cdot \frac{x}{z} f_g\left(\frac{x}{z}, \mu^2\right). \quad (15)$$

The cross section (13) with ‘‘unPDFs’’ (15) contains the collinear divergence at $t_{1,2} \rightarrow 0$ and infrared (IR) divergence at $z_{1,2} \rightarrow 1$. To regularize the latter, we observe that the mMRK expression (11) can be expected to give a reasonable approximation for the exact matrix element only in the rapidity-ordered part of the phase space, where $\Delta y_1 > 0$ and $\Delta y_2 > 0$. The cutoff on $z_{1,2}$ follows from these conditions,

$$z_{1,2} < 1 - \Delta_{\text{KMR}}(t_{1,2}, \mu^2), \quad (16)$$

where $\Delta_{\text{KMR}}(t, \mu^2) = \sqrt{t}/(\sqrt{\mu^2} + \sqrt{t})$, and we have taken into account that $\mu^2 \sim M_{T,A}^2$. The collinear singularity is regularized by the Sudakov form factor,

$$\begin{aligned} T_i(t, \mu^2) &= \exp\left[-\int_t^{\mu^2} \frac{dt' \alpha_s(t')}{t' 2\pi} \right. \\ &\left. \times \sum_{j=q,\bar{q},g} \int_0^1 dz z \cdot P_{ji}(z) \theta(1 - \Delta_{\text{KMR}}(t', \mu^2) - z)\right], \end{aligned} \quad (17)$$

which resums the doubly logarithmic corrections $\sim \log^2(t/\mu^2)$ in the Leading Logarithmic Approximation in a way similar to what is done in the standard PS [27].

The final form of our unPDF is

$$\begin{aligned} \Phi_i(x, t, \mu^2) &= \frac{T_i(t, \mu^2) \alpha_s(t)}{t 2\pi} \sum_{j=q,\bar{q},g} \int_x^1 dz P_{ij}(z) \cdot \frac{x}{z} f_j\left(\frac{x}{z}, t\right) \\ &\cdot \theta(1 - \Delta_{\text{KMR}}(t, \mu^2) - z), \end{aligned} \quad (18)$$

which coincides with the Kimber, Martin, and Ryskin (KMR) unPDF [28]. The KMR unPDF is actively used in the phenomenological studies employing k_T -factorization, but to our knowledge, the reasoning above is the first systematic attempt to uncover its relationships with the MRK limit of the QCD amplitudes.

The KMR unPDF approximately (see Sec. 2 of Ref. [29] for further details) satisfies the following normalization condition:

$$\int_0^{\mu^2} dt \Phi_i(x, t, \mu^2) = x f_i(x, \mu^2), \quad (19)$$

which ensures the normalization for the single-scale observables, such as the proton structure functions or $d\sigma/dQ^2 dy$ cross section in the Drell-Yan process, on the corresponding LO CPM results up to power-suppressed corrections and terms of the NLO in α_s . Results for multiscale observables in the PRA are significantly different than those in the CPM, due to the nonzero transverse momenta of partons in the initial state.

The main difference of the PRA from the multitude of studies in the k_T -factorization, such as Ref. [15], is the application of matrix elements with off-shell initial-state partons (Reggeized quarks and gluons) from Lipatov’s EFT [19,20], which allows one to study the arbitrary processes involving the non-Abelian structure of QCD without violation of gauge invariance due to the nonzero virtuality of initial-state partons. This approach, together with the KMR unPDF, gives stable and consistent results in a wide range of phenomenological applications, which include the description of the angular correlations of dijets [30], b -jets [31], charmed [32,33] and bottom-flavored [34] mesons, different multiscale observables in hadroproduction of diphotons [26] and photoproduction of photon + jet pairs [35], as well as some other examples.

Recently, the new approach to derive gauge-invariant scattering amplitudes with off-shell initial-state partons,

using the spinor-helicity techniques and Britto-Cachazo-Feng-Witten-like recursion relations for such amplitudes, was introduced in Refs. [36,37]. This formalism is equivalent to Lipatov's EFT at the tree level, but for some observables, e.g., related with heavy quarkonia, or for the generalization of the formalism to NLO, the explicit Feynman rules and the structure of EFT are more convenient.

III. LO PRA MERGED WITH TREE-LEVEL NLO CORRECTIONS

Let us consider the kinematic conditions of a measurement in Ref. [3]. In this experiment, the events with at least one jet having $p_T^{\text{jet}} > p_{TL}^{\text{min}}$ have been recorded in pp -collisions at $\sqrt{S} = 7$ TeV, and the semileptonic decays of B -hadrons reconstructed in these events, through the decay vertices, which are displaced with respect to the primary pp -collision vertex. The B -hadron is required to have $p_{TB} > p_{TB}^{\text{min}} = 15$ GeV, while three data samples are presented in Ref. [3] for three values of $p_{TL}^{\text{min}} = 56, 84,$ and 120 GeV. The rapidities of B -hadrons are constrained to be $|y_B| < y_B^{\text{max}} = 2$, while the leading jet is searched for in a somewhat wider domain $|y_{\text{jet}}| < y_{\text{jet}}^{\text{max}} = 3$.

The leading jet, reconstructed in this experiment, sets the hard scale of the event. Two possibilities should be considered: the first one is that the jet originating from the b -quark or \bar{b} -antiquark is the leading one, and the second option is that some gluon or light-quark jet is leading in p_T , and jets originating from b or \bar{b} are subleading. Observables with such kinematic constraints on the QCD radiation are difficult to study in k_T -factorization, because the radiation of additional hard partons is already taken into account in the unPDFs, and the jet originating from the unPDF could happen to be the leading one.

One can easily estimate the distribution of additional jets in rapidity, using the KMR model for unPDFs (18). The variable z is related with rapidity (y) of the parton, emitted in the last step of the parton cascade, as follows:

$$z(y) = \left(1 + \frac{\sqrt{t}}{x\sqrt{S}} e^y\right)^{-1},$$

so, starting from Eq. (18) one can derive the distribution integrated over t from some scale t_0 up to μ^2 , but unintegrated over y : $G_i(x, y, t_0, \mu^2)$. Representative plots of this distribution for the case of P_{gg} -splitting only are shown in Fig. 4 for some values of scales typical for the process under consideration. The LO PDFs from the MSTW-2008 set [38] have been used to produce this plot.

From Fig. 4 it is clear that in the KMR model, the majority of the hardest ISR jets with $\mathbf{k}_T^2 \sim \mu^2$ lie within the rapidity interval $|y| < 3$ if the particles produced in the primary hard process have rapidities close to zero. Therefore these jets can be identified as the leading ones. But the kinematic approximations, which have been made

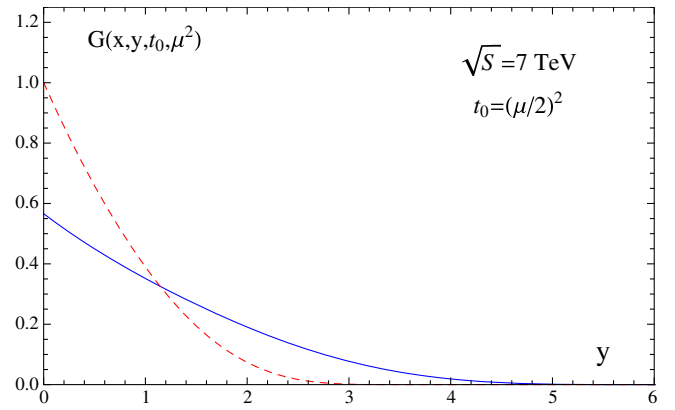


FIG. 4. Distribution in the rapidity of gluon jets with $|\mathbf{k}_T| > \mu/2$ from the last stage of the parton cascade, as given by the KMR model (18). The solid line represents $\mu^2 = 10^3$ GeV²; the dashed line represents $\mu^2 = 10^5$ GeV². Both plots are normalized to the common integral; the scale of the G -axis is arbitrary. For both distributions, $x = \mu/\sqrt{S}$; i.e., the rapidity of the hard process is zero.

in the derivation of the factorization formula, are least reliable in this region of phase space, and hence the poor agreement with data is to be expected. To avoid the above-mentioned problem, we will merge the LO PRA description of events with the leading $b(\bar{b})$ -jets with events triggered by the leading gluon jet, originating from the exact $2 \rightarrow 3$ NLO PRA matrix element.

The LO [$O(\alpha_s^2)$] subprocess, which we will take into account, is

$$R_+(q_1) + R_-(q_2) \rightarrow b(q_3) (\rightarrow B(p_{TB})) + \bar{b}(q_4) (\rightarrow \bar{B}(p_{T\bar{B}})), \quad (20)$$

where the hadronization of $b(\bar{b})$ -quarks into the $B(\bar{B})$ mesons is described by the set of universal, scale-dependent parton-to-hadron fragmentation functions, fitted on the world data on the B -hadron production in the e^+e^- -annihilation in Ref. [39].

The following kinematic cuts are applied to the LO subprocess (20):

- (1) Both B and \bar{B} mesons are required to have $|y_B| < y_B^{\text{max}}$ and $\min(p_{TB}, p_{T\bar{B}}) > p_{TB}^{\text{min}}$.
- (2) If the distance between three-momenta \mathbf{q}_3 and \mathbf{q}_4 in the $(\Delta y, \Delta\phi)$ -plane is $\Delta R_{34} = \sqrt{\Delta y_{34}^2 + \Delta\phi_{34}^2} > \Delta R_{\text{exp}} = 0.5$, then the b and \bar{b} jets are resolved separately and we define $p_{TL} = \max(|\mathbf{q}_{T3}|, |\mathbf{q}_{T4}|)$.
- (3) If $\Delta R_{34} < \Delta R_{\text{exp}}$, then $p_{TL} = |\mathbf{q}_{T3} + \mathbf{q}_{T4}|$, according to the anti- k_T jet clustering algorithm [40].
- (4) The MC event is *accepted* if $\max(|\mathbf{q}_{T1}|, |\mathbf{q}_{T2}|) < p_{TL}$ and $p_{TL} > p_{TL}^{\text{min}}$.

The set of Feynman diagrams for the subprocess (20) is presented in Fig. 5. The convenient expression for the squared amplitude of this subprocess with massless quarks

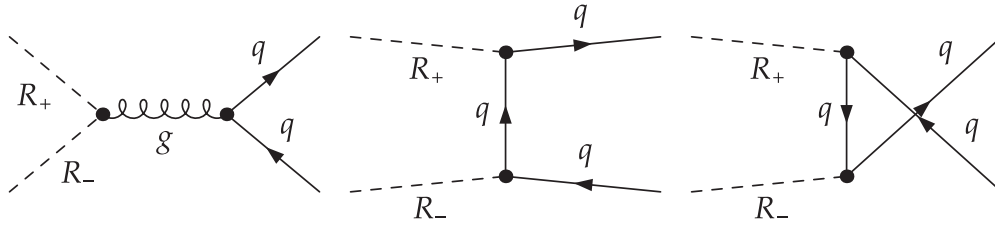


FIG. 5. The Feynman diagrams of Lipatov's EFT for the Reggeized amplitude of subprocess $R_+ + R_- \rightarrow b + \bar{b}$.

can be found in Ref. [30]. Due to the Ward identities of Ref. [23], this amplitude coincides with the amplitude that can be obtained in the “old k_T -factorization” prescription, i.e., by substituting the polarization vectors of initial-state gluons in the usual $gg \rightarrow q\bar{q}$ amplitude by $q_{T1,2}^\mu/|\mathbf{q}_{T1,2}|$.

The NLO [$O(\alpha_s^3)$] subprocess is

$$R_+(q_1) + R_-(q_2) \rightarrow b(q_3)(\rightarrow B(p_{TB})) + \bar{b}(q_4)(\rightarrow \bar{B}(p_{T\bar{B}})) + g(q_5), \quad (21)$$

and the following kinematic constraints are applied in the calculation of this contribution:

- (1) Both B and \bar{B} mesons are required to have $|y_B| < y_B^{\max}$ and $\min(p_{TB}, p_{T\bar{B}}) > p_{TB}^{\min}$.
- (2) The gluon jet is the leading one: $p_{TL} = |\mathbf{q}_{T5}|$, $\max(|\mathbf{q}_{T1}|, |\mathbf{q}_{T2}|, |\mathbf{q}_{T3}|, |\mathbf{q}_{T4}|) < p_{TL}$, and $p_{TL} > p_{TL}^{\min}$.
- (3) Rapidity of the gluon is required to be $|y_5| < y_{\text{jet}}^{\max}$. The gluon jet is isolated: $\Delta R_{35} > \Delta R_{\text{exp}}$ and $\Delta R_{45} > \Delta R_{\text{exp}}$.

Furthermore, since the matrix elements for both subprocesses (20) and (21) are taken in the approximation of massless b -quarks, the corresponding final-state collinear singularity is regularized by the condition $(q_3 + q_4)^2 > 4m_b^2$, where $m_b = 4.5$ GeV.

A few comments are in order. For both subprocesses (20) and (21), transverse momenta of jets from the unPDFs are constrained to be subleading. In such a way we avoid the double-counting of the leading emissions between the LO and NLO contributions and additional subtractions are not needed. This is in contrast to the observables fully inclusive in the QCD radiation [26], where the double-counting subtractions between LO and NLO terms have to be done. For the reader's convenience, we also illustrate the complementarity of phase spaces for the LO contribution (20) and NLO contribution (21) in Fig. 6. One can observe that the above-described kinematic cuts clearly separate events coming from the $2 \rightarrow 2$ subprocess from the events generated by the $2 \rightarrow 3$ subprocess.

Another comment concerns the isolation condition for the leading gluon jet in the NLO contribution (21). This condition regularizes the collinear singularity between the final-state gluon and $b(\bar{b})$ -quark. In the full NLO calculation, this singularity will be absorbed by the renormalization of the parton-to-meson fragmentation

function and also partially canceled by the loop correction, thus leaving some finite contribution, but since in the case of subprocess (21) the gluon is required to be harder than b or \bar{b} -quarks, this finite contribution will be proportional to the $P_{gq}(z) = C_F(1 + (1 - z)^2)/z$ splitting function at $z \rightarrow 1$, so we do not expect the logarithmically enhanced contributions from this region of the phase space.

In more standard calculations that merge the MC PS with higher-order matrix elements [7,8], the variable, sometimes called the “merging scale,” appears. This variable controls the separation of the emissions generated by the PS from the emissions from the NLO matrix element. In our case, the boundary between the $2 \rightarrow 2$ and $2 \rightarrow 3$ regions in Fig. 6 is the analog of the merging scale. Approximate cancellation of the dependence of the cross section from the merging prescription then follows from the fact that if we move the boundary toward the $p_T^{b\text{-jet}}$ axis in Fig. 6, then the kinematics of the emission of additional partons becomes closer to the MRK and eventually to the collinear limits, so that the mMRK approximation, formulated in Sec. II, describes the exact $2 \rightarrow 3$ matrix element better and better.

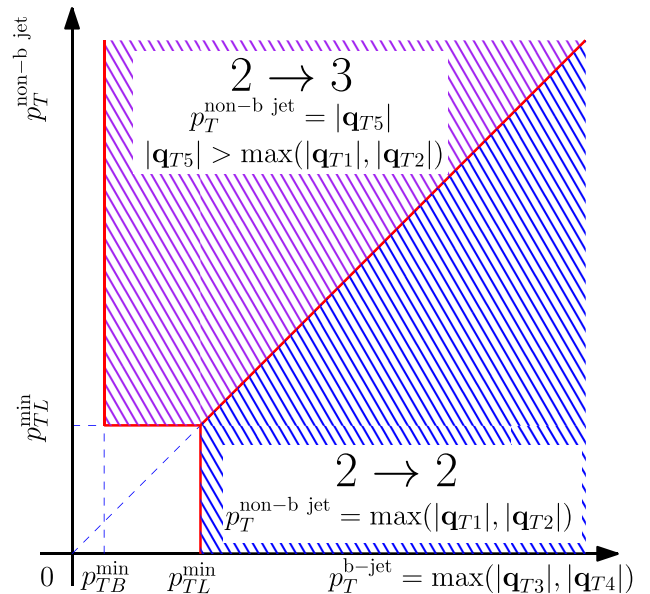


FIG. 6. The kinematic cuts for the $2 \rightarrow 2$ contribution (20) and $2 \rightarrow 3$ contribution (21) in the space of transverse momentum of the leading b -jet in the event ($p_T^{b\text{-jet}}$) vs transverse momentum of the leading light-quark/gluon jet in the same event ($p_T^{\text{non-}b\text{-jet}}$).

In fact, the merging prescription described above is probably optimal, because it lies on the edge of applicability of the mMRK approximation. Thus, the full power of the LO PRA approximation is exploited and it is substituted by the NLO matrix element only when the underlying mMRK approximation breaks down.

The set of Feynman diagrams for the amplitude of subprocess (21) is presented in Fig. 7. We generate this amplitude, using our model file `ReggeQCD`, which implements the Feynman rules of Lipatov's EFT in `FeynArts` [41]. The squared amplitude is computed using the `FormCalc` [42] package and has been compared numerically with the squared amplitude, obtained by the methods of Refs. [36,37]. Our results and the results of Refs. [36,37] agree up to machine precision. Apart from the Feynman rules, depicted in Figs. 1 and 2, the `ReggeQCD` package contains all Feynman rules, which are needed to generate an arbitrary PRA amplitude with Reggeized gluons or quarks in the initial state and up to three quarks, gluons, or photons in the final state. We are planning to publish the `ReggeQCD` model file in a separate paper [43]. The FORTRAN code for the squared amplitudes of the processes (20) and (21) is available from the authors by request.

As stated above, we will use the fragmentation model to describe the hadronization of b -quarks into B -hadrons, so the observable cross section is

$$\frac{d\sigma_{\text{obs}}}{dy_B dy_{\bar{B}} d\Delta\phi} = \int_{p_{TB}^{\text{min}}}^{\infty} dp_{TB} \int_{p_{T\bar{B}}^{\text{min}}}^{\infty} dp_{T\bar{B}} \int_0^1 \frac{dz_1}{z_1} D_{B/b}(z_1, \mu^2) \times \int_0^1 \frac{dz_2}{z_2} D_{\bar{B}/\bar{b}}(z_2, \mu^2) \frac{d\sigma_{b\bar{b}}}{dq_{T3} dq_{T4} dy_3 dy_4 d\Delta\phi}, \quad (22)$$

where $\Delta\phi = \Delta\phi_{34}$, $D_{B/b}(z, \mu^2)$ are the fragmentation functions [39], and $q_{T3} = |\mathbf{q}_{T3}| = p_{TB}/z_1$, $q_{T4} = |\mathbf{q}_{T4}| = p_{T\bar{B}}/z_2$, $y_3 = y_B$, and $y_4 = y_{\bar{B}}$. To simplify the numerical calculations, it is very convenient to integrate over $q_{T3,4}$ instead of p_{TB} and $p_{T\bar{B}}$ in Eq. (22); then all the dependence of the cross section on fragmentation functions can be absorbed into the following measurement function:

$$\Theta(\tilde{z}, \mu^2) = \begin{cases} \int_{1/\tilde{z}}^1 dz D_{B/q}(z, \mu^2) & \text{if } \tilde{z} > 1, \\ 0 & \text{otherwise,} \end{cases} \quad (23)$$

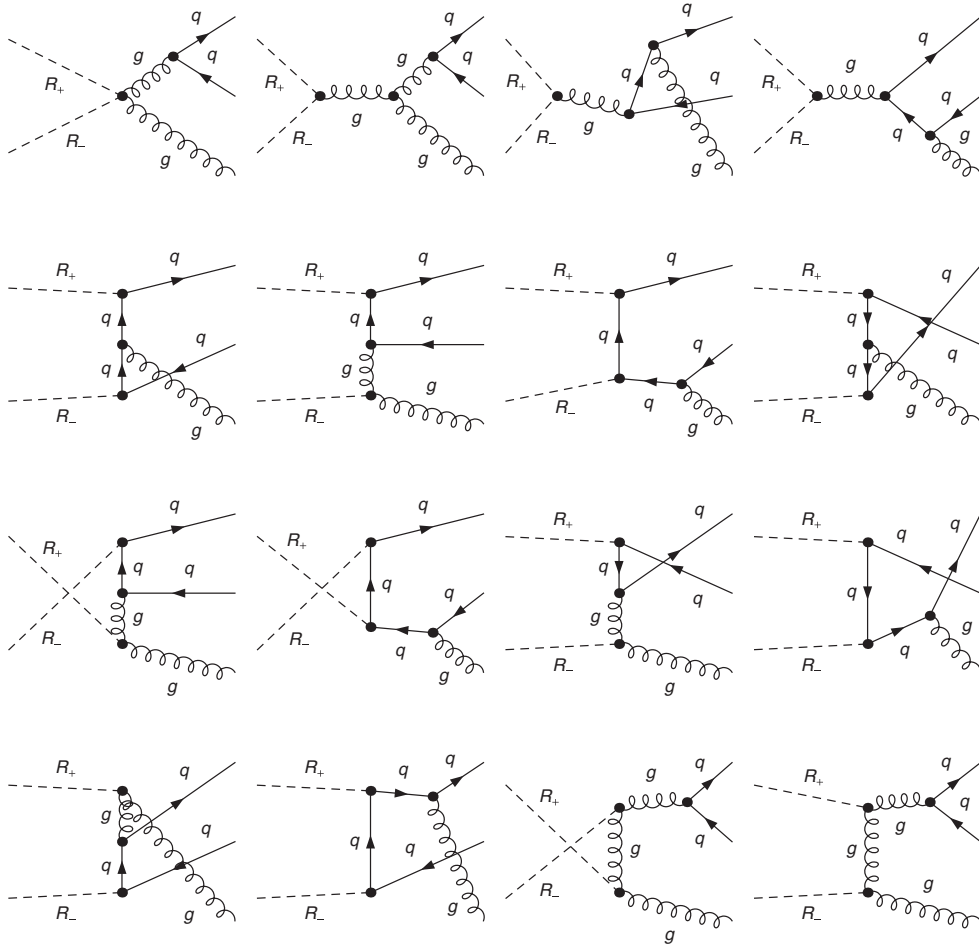


FIG. 7. The Feynman diagrams of Lipatov's EFT for the Reggeized amplitude of subprocess $R_+ + R_- \rightarrow b + \bar{b} + g$.

which can be efficiently computed and tabulated in advance, therefore reducing the dimension of phase-space integrals by 2. Then the master formula for the cross section of the $2 \rightarrow 2$ subprocess (20) in the PRA takes the form

$$\begin{aligned} \frac{d\sigma_{\text{obs}}^{(2\rightarrow 2)}}{dy_B dy_{\bar{B}} d\Delta\phi} &= \int_0^\infty dq_{T3} dq_{T4} \cdot \Theta\left(\frac{q_{T3}}{p_{TB}^{\text{min}}}, \mu^2\right) \Theta\left(\frac{q_{T4}}{p_{TB}^{\text{min}}}, \mu^2\right) \\ &\times \int_0^\infty dt_1 \int_0^{2\pi} d\phi_1 \Phi_g(x_1, t_1, \mu^2) \\ &\times \Phi_g(x_2, t_2, \mu^2) \cdot \frac{q_{T3} q_{T4} |\mathcal{A}_{\text{PRA}}^{(2\rightarrow 2)}|^2}{2(2\pi)^3 (Sx_1 x_2)^2} \cdot \theta_{\text{cuts}}^{(2\rightarrow 2)}, \end{aligned} \quad (24)$$

where ϕ_1 is the azimuthal angle between the vector \mathbf{q}_{T1} and \mathbf{q}_{T3} , $t_2 = |\mathbf{q}_{T3} + \mathbf{q}_{T4} - \mathbf{q}_{T1}|$, $x_1 = (q_3^+ + q_4^+)/\sqrt{S}$, $x_2 = (q_3^- + q_4^-)/\sqrt{S}$, and the theta function $\theta_{\text{cuts}}^{(2\rightarrow 2)}$ implements the kinematic constraints for the $2 \rightarrow 2$ process, described above. Analogously, the formula for the differential cross section of the $2 \rightarrow 3$ process (21) reads

$$\begin{aligned} \frac{d\sigma_{\text{obs}}^{(2\rightarrow 3)}}{dy_B dy_{\bar{B}} d\Delta\phi dy_5} &= \int_0^\infty dq_{T3} dq_{T4} \cdot \Theta\left(\frac{q_{T3}}{p_{TB}^{\text{min}}}, \mu^2\right) \Theta\left(\frac{q_{T4}}{p_{TB}^{\text{min}}}, \mu^2\right) \\ &\times \int_0^\infty dt_1 dt_2 \int_0^{2\pi} d\phi_1 d\phi_2 \Phi_g(x_1, t_1, \mu^2) \\ &\times \Phi_g(x_2, t_2, \mu^2) \cdot \frac{q_{T3} q_{T4} |\mathcal{A}_{\text{PRA}}^{(2\rightarrow 3)}|^2}{8(2\pi)^6 (Sx_1 x_2)^2} \cdot \theta_{\text{cuts}}^{(2\rightarrow 3)}, \end{aligned} \quad (25)$$

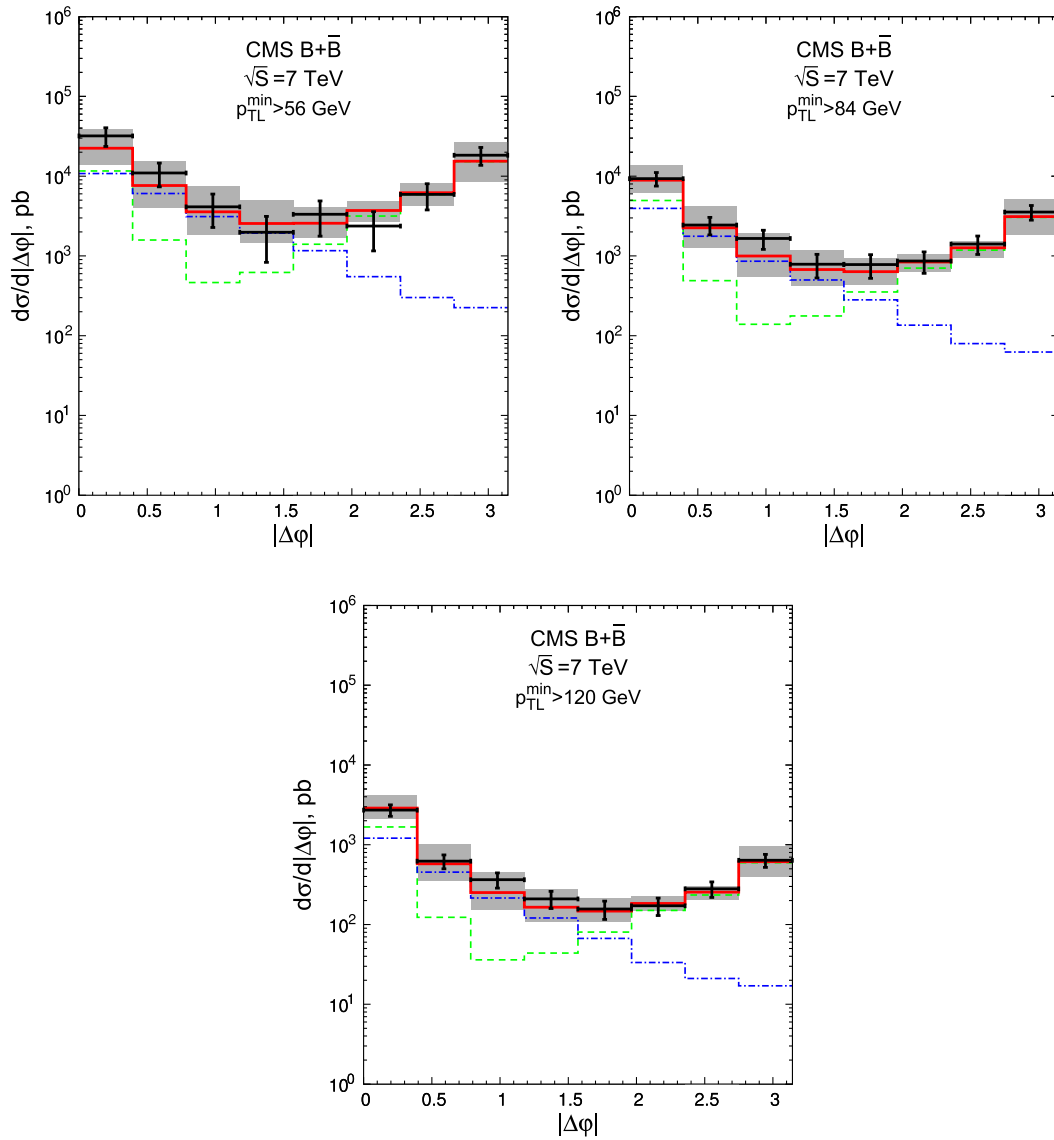


FIG. 8. Comparison of the predictions for $\Delta\phi$ -spectra of $B\bar{B}$ -pairs with the CMS data [3]. The dashed, dashed-dotted, and solid lines represent the contribution of the LO subprocess (20), contribution of the NLO subprocess (21), and sum of the LO and NLO contributions, respectively.

where ϕ_2 is the azimuthal angle between the vectors \mathbf{q}_{T2} , and \mathbf{q}_{T3} , $\mathbf{q}_{T5} = \mathbf{q}_{T1} + \mathbf{q}_{T2} - \mathbf{q}_{T3} - \mathbf{q}_{T4}$, $x_1 = (q_3^+ + q_4^+ + q_5^+)/\sqrt{S}$, $x_2 = (q_3^- + q_4^- + q_5^-)/\sqrt{S}$; and the theta function θ^{cuts} implements kinematic cuts for the $2 \rightarrow 3$ process, described after Eq. (21).

IV. NUMERICAL RESULTS FOR $B\bar{B}$ -CORRELATION OBSERVABLES

Now we are in a position to compare our numerical results, obtained in the approximation formulated in Sec. III of the present paper, to the experimental data of Ref. [3]. Experimental uncertainties, related with the shape of $\Delta\phi$ and $\Delta R = \Delta R_{34}$ distributions, are relatively small (~ 20 – 30%). They are indicated by the error bars in

Figs. 8 and 9. However, an additional uncertainty in the absolute normalization of the cross sections $\approx \pm 47\%$ is reported in Ref. [3], but it is not included in the error bars of the experimental points in Figs. 8 and 9 or in the plots presented in the experimental paper. Taking this large uncertainty into account, it is reasonable to consider the overall normalization of the cross section to be a free parameter, which is also the case in MC simulations presented in Ref. [3]. Following this route we find that to obtain a very good agreement of the central curve of our predictions both with the shape and normalization of all experimental spectra we have to multiply all our predictions on the universal factor ≈ 0.4 . Since the major part of the reported normalization uncertainty is due to the uncertainty in the efficiency of identification of B -mesons, our finding

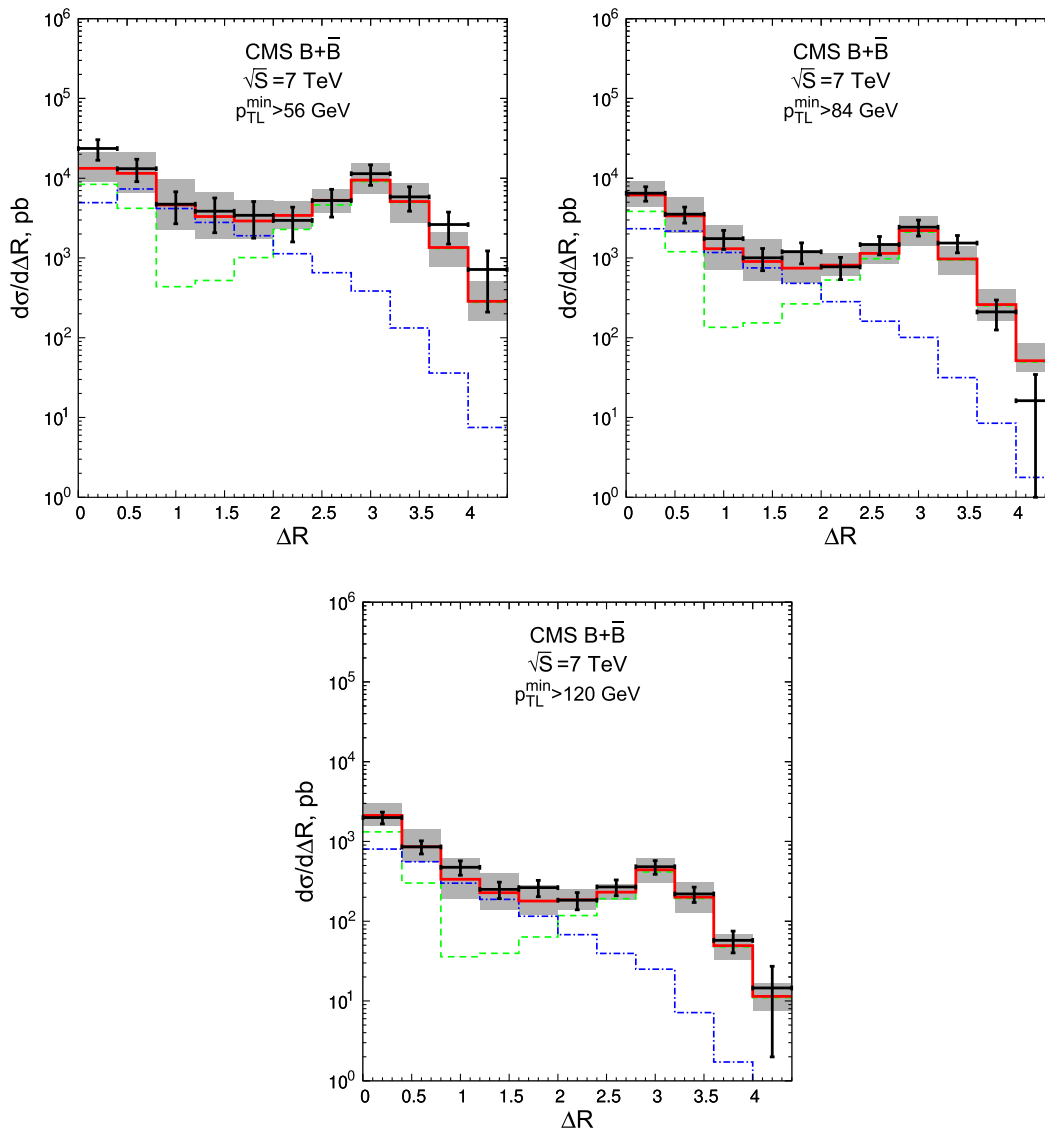


FIG. 9. Comparison of the predictions for ΔR -spectra of $B\bar{B}$ -pairs with the CMS data [3]. Notation for the histograms is the same as in Fig. 8.

seems to support the assumption that the B -meson reconstruction efficiency is largely independent from the kinematics of the leading jet, and in particular, from the value of p_{TL}^{\min} . In the plots below, we show theoretical predictions multiplied by the above-mentioned factor; however, our default result is also compatible with experiment, if one takes into account full experimental uncertainties and the scale uncertainty of our predictions.

In Figs. 8 and 9 we present the comparison of our predictions with $\Delta\phi$ and ΔR spectra from Ref. [3]. Apart from the above-mentioned overall normalization uncertainty, our model does not contain any free parameters. To generate the gluon unPDF, according to Eq. (18) we use the LO PDFs from the MSTW-2008 set [38]. We also use the value of $\alpha_s(M_Z) = 0.1394$ from the PDF fit. In both LO (20) and NLO (21) contributions we set the renormalization

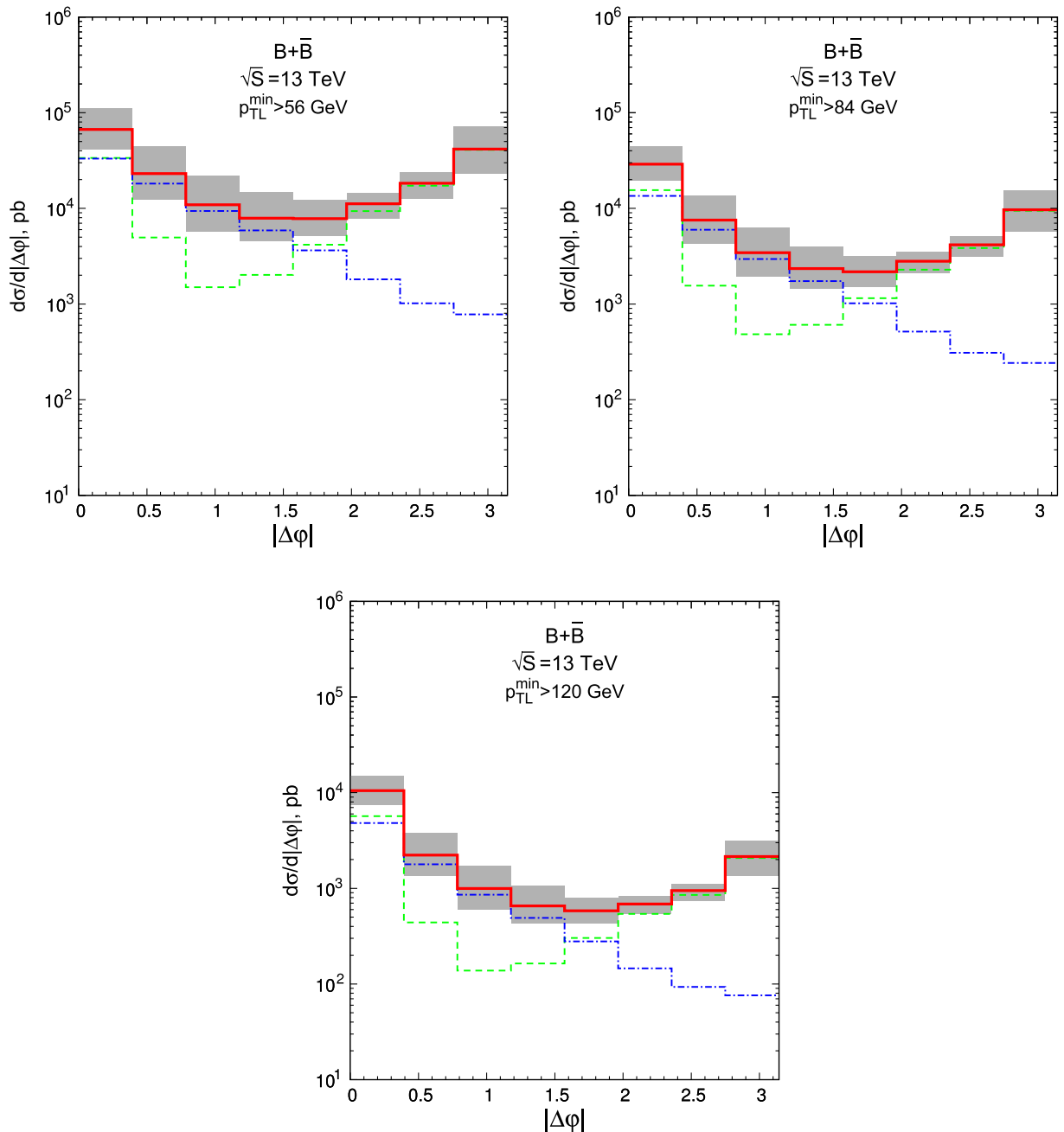


FIG. 10. Predictions for the $d\sigma/d\Delta\phi$ -spectra $\sqrt{S} = 13$ TeV for the same kinematic cuts as in Ref. [3]. Notation for the histograms is the same as in Fig. 8.

and factorization scales to be equal to the p_T of the leading jet: $\mu_R = \mu_F = \xi p_{TL}$, where $\xi = 1$ for the central lines of our predictions, and we vary $1/2 < \xi < 2$ to estimate the scale uncertainty of our prediction, which is shown in the following figures by the gray band. All numerical calculations have been performed using the adaptive MC integration routines from the CUBA library [44], mostly using the SUAVE algorithm, but with the cross-checks

against the results obtained by the VEGAS and DIVONNE routines.

The shape of measured distributions, both in $\Delta\phi$ and ΔR , agrees with our theoretical predictions within the experimental uncertainty. Also, our model correctly describes the dependence of the cross section on the p_{TL}^{\min} cut.

Recently, the ATLAS Collaboration performed a measurement of a large set of correlation observables for

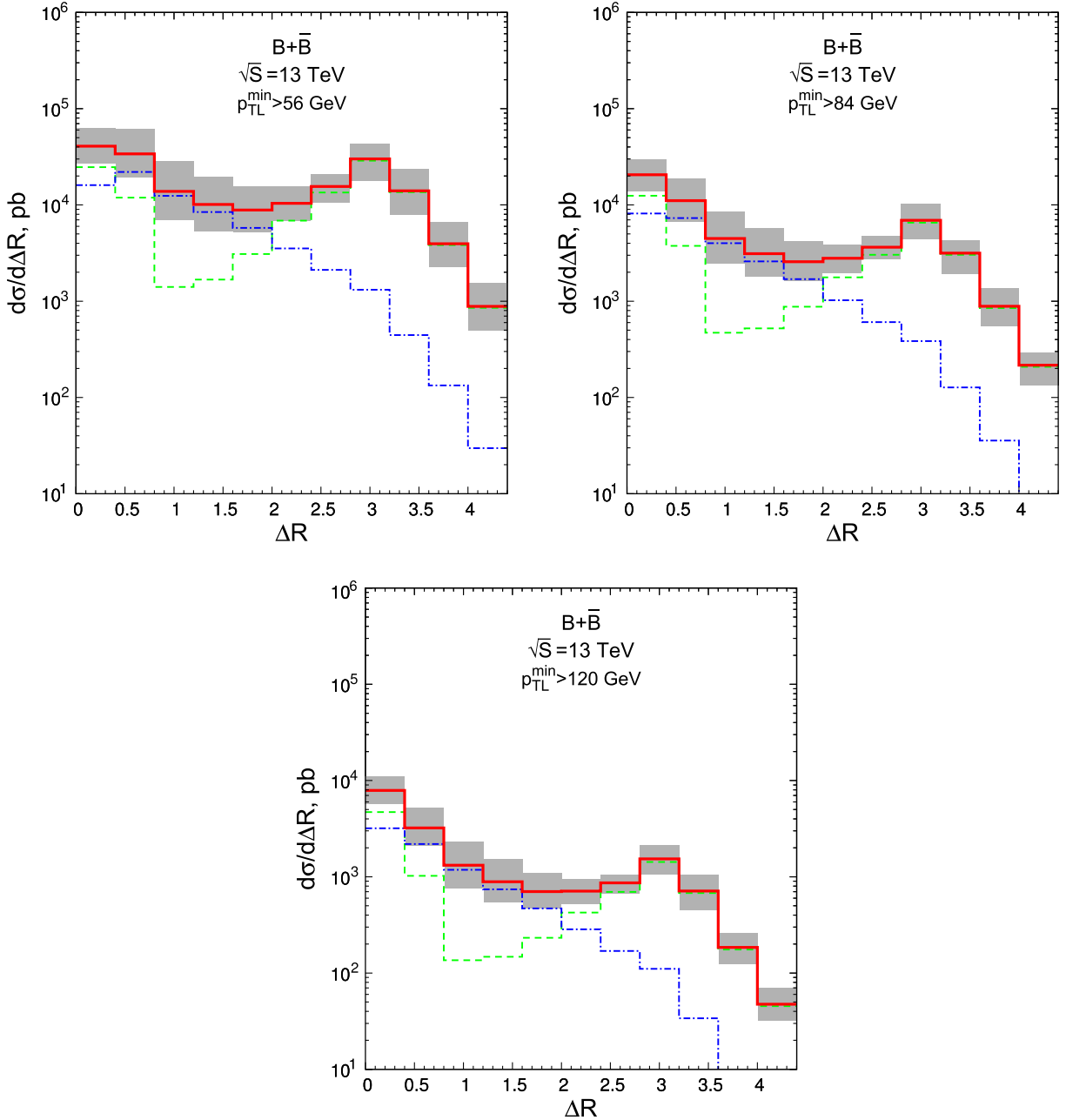


FIG. 11. Predictions for the $d\sigma/d\Delta R$ -spectra $\sqrt{S} = 13$ TeV for the same kinematic cuts as in Ref. [3]. Notation for the histograms is the same as in Fig. 8.

b -hadron pair production in the pp -collisions at $\sqrt{S} = 8$ TeV [16]. Comparison of predictions of our model to the results of this measurement requires the detailed MC modeling of the decays b -hadron $\rightarrow J/\psi(\rightarrow \mu^+\mu^-) + X$ and b -hadron $\rightarrow \mu + X$ which has been selected for the analysis in the Ref. [16]. This work is in progress and will be the subject of a future publication.

Our predictions for the $d\sigma/d\Delta\phi$ and $d\sigma/d\Delta R$ spectra at $\sqrt{S} = 13$ TeV are presented in Figs. 10 and 11 for the same kinematic cuts as in Ref. [3]. Also in Figs. 12 and 13 we provide predictions for the ratios of $\Delta\phi$ and ΔR spectra at

different energies, as proposed in Ref. [45]. The primary advantage of such observables is that the theoretical scale uncertainty mostly cancels in the ratio, leading to a more precise prediction. The residual $\Delta\phi$ and ΔR dependence of the ratio arises in the interplay between the x -dependence of PDFs and the dynamics of emissions of additional hard radiation, therefore probing the physics of interest for the PRA. Measurements of such observables at the LHC will present an important challenge for state-of-the-art calculations in perturbative QCD and tuning of the MC event generators.

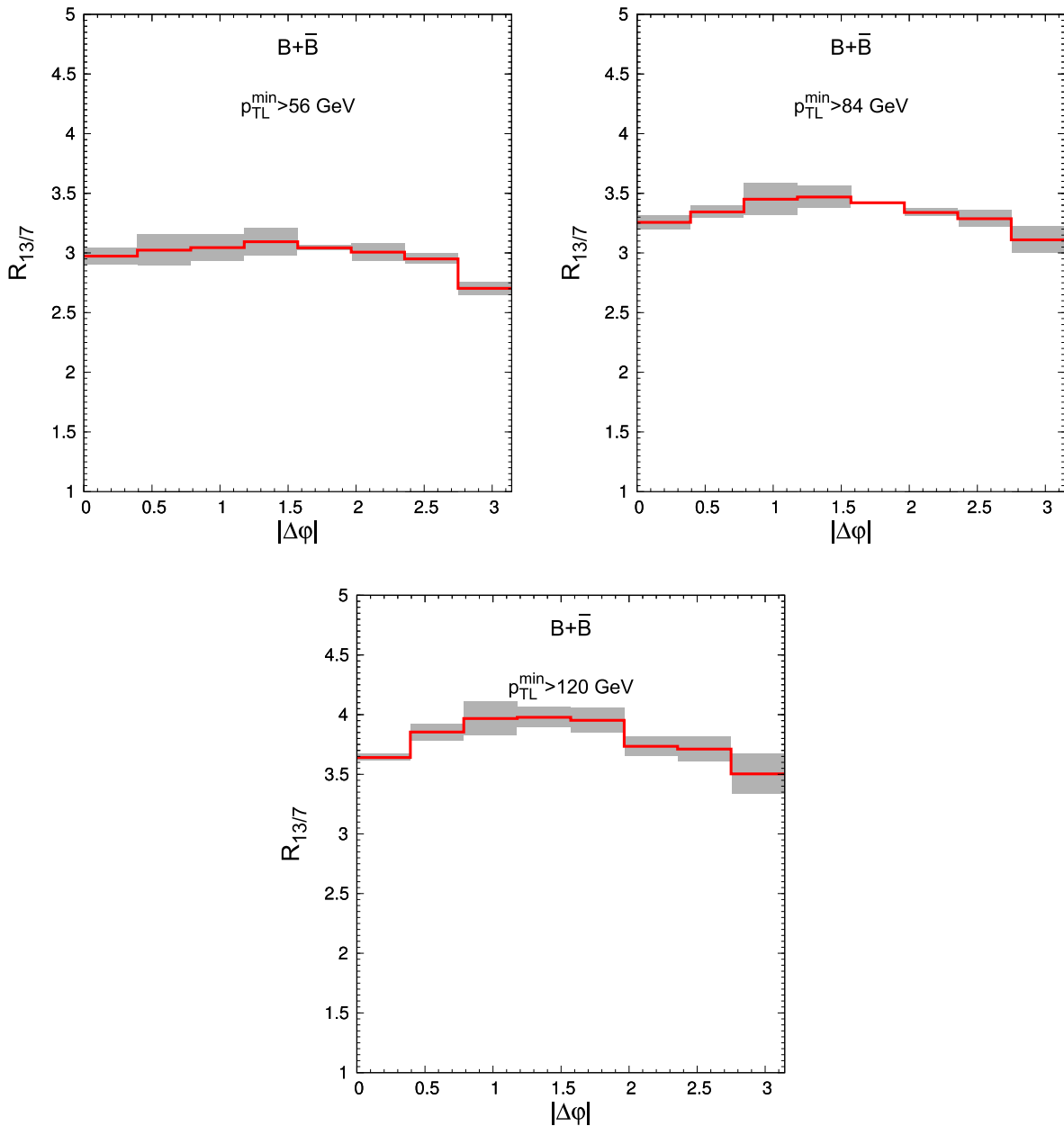


FIG. 12. Predictions for the ratio of $d\sigma/d\Delta\phi$ -spectra at $\sqrt{S} = 13$ TeV and $\sqrt{S} = 7$ TeV for the same kinematic cuts as in Ref. [3].

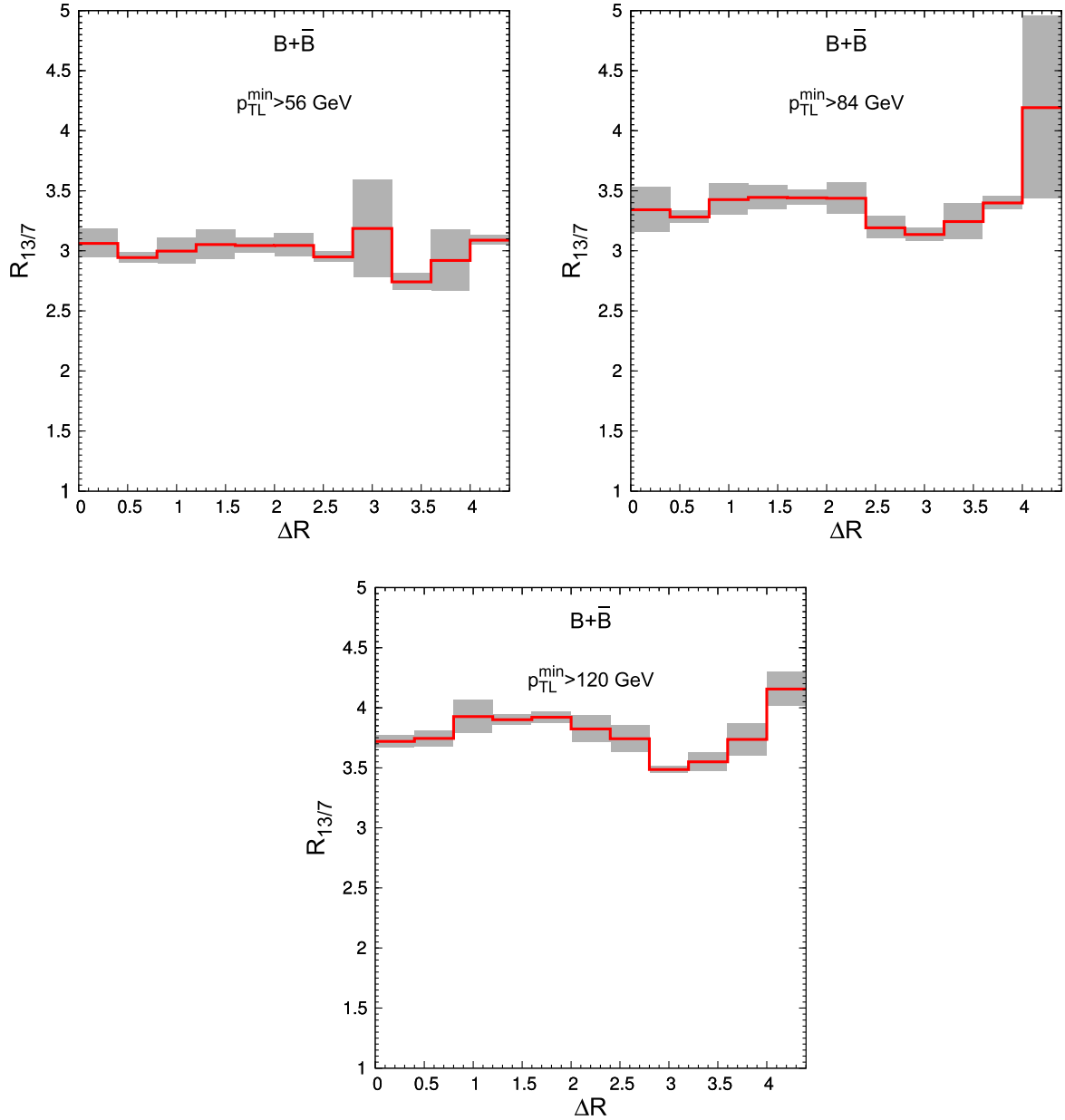


FIG. 13. Predictions for the ratio of $d\sigma/d\Delta R$ -spectra at $\sqrt{S} = 13$ TeV and $\sqrt{S} = 7$ TeV for the same kinematic cuts as in Ref. [3].

V. CONCLUSIONS

In the present paper, the example of $B\bar{B}$ -azimuthal decorrelations has been used to show how the contributions of the $2 \rightarrow 2$ and $2 \rightarrow 3$ processes in the PRA can be consistently taken together to describe multiscale correlational observables in the presence of experimental constraints on additional QCD radiation. Our numerical results agree well with the experimental data of Ref. [3], up to a common normalization factor. The predictions for $\sqrt{S} = 13$ TeV have been provided. Also, the foundations of the parton Reggeization approach were reviewed in Sec. II, and the relation of the PRA with collinear and

multi-Regge limits of scattering amplitudes in QCD has been highlighted.

ACKNOWLEDGMENTS

We are grateful to A. van Hameren for help in the comparison of squared amplitudes obtained in the PRA with ones obtained using the recursion techniques of Refs. [36,37]. The work was supported by the Ministry of Education and Science of Russia under the Competitiveness Enhancement Program of Samara University for 2013–2020, project 3.5093.2017/8.9. The Feynman diagrams in Figs. 1, 2, and 3 were made using JAXODRAW [46].

- [1] T. Aaltonen *et al.* (CDF Collaboration), Measurement of the $b\bar{b}$ cross section using a dedicated trigger in $p\bar{p}$ collisions at 1.96 TeV, CDF note 8939, 2007, www.cdf.fnal.gov/physics/new/qcd/bb_SVT_07/cdf8939_bbjet_highpt_public.ps.
- [2] G. Aad *et al.* (ATLAS Collaboration), Measurement of the inclusive and dijet cross-sections of b^- jets in pp collisions at $\sqrt{s} = 7$ TeV with the ATLAS detector, *Eur. Phys. J. C* **71**, 1846 (2011).
- [3] V. Khachatryan *et al.* (CMS Collaboration), Measurement of $B\bar{B}$ angular correlations based on secondary vertex reconstruction at $\sqrt{s} = 7$ TeV, *J. High Energy Phys.* **03** (2011) 136.
- [4] R. Corke and T. Sjostrand, Interleaved parton showers and tuning prospects, *J. High Energy Phys.* **03** (2011) 032.
- [5] S. Frixione and B.R. Webber, Matching NLO QCD computations and parton shower simulations, *J. High Energy Phys.* **06** (2002) 029.
- [6] S. Alioli, P. Nason, C. Oleari, and E. Re, A general framework for implementing NLO calculations in shower Monte Carlo programs: The POWHEG BOX, *J. High Energy Phys.* **06** (2010) 043.
- [7] S. Catani, F. Krauss, R. Kuhn, and B.R. Webber, QCD matrix elements + parton showers, *J. High Energy Phys.* **11** (2001) 063.
- [8] M.H. Seymour, Matrix element corrections to parton shower algorithms, *Comput. Phys. Commun.* **90**, 95 (1995).
- [9] T. Sjostrand, S. Mrenna, and P.Z. Skands, PYTHIA 6.4 physics and manual, *J. High Energy Phys.* **05** (2006) 026.
- [10] G. Corcella, I.G. Knowles, G. Marchesini, S. Moretti, K. Odagiri, P. Richardson, M.H. Seymour, and B.R. Webber, HERWIG 6: An event generator for hadron emission reactions with interfering gluons (including supersymmetric processes), *J. High Energy Phys.* **01** (2001) 010.
- [11] J. Alwall, P. Demin, S. de Visscher, R. Frederix, M. Herquet, F. Maltoni, T. Plehn, D.L. Rainwater, and T. Stelzer, MadGraph/MadEvent v4: The New Web Generation, *J. High Energy Phys.* **09** (2007) 028.
- [12] F. Maltoni and T. Stelzer, MadEvent: Automatic event generation with MadGraph, *J. High Energy Phys.* **02** (2003) 027.
- [13] H. Jung and G.P. Salam, Hadronic final state predictions from CCFM: The hadron level Monte Carlo generator CASCADE, *Eur. Phys. J. C* **19**, 351 (2001).
- [14] M. Ciafaloni, Gluon saturation beyond (naive) leading logs, *Nucl. Phys.* **B296**, 49 (1988); S. Catani, F. Fiorani, and G. Marchesini, Small-x behaviour of initial state radiation in perturbative QCD, *Nucl. Phys.* **B336**, 18 (1990); QCD coherence in initial state radiation, *Phys. Lett. B* **234**, 339 (1990); G. Marchesini, QCD coherence in the structure function and associated distributions at small x, *Nucl. Phys.* **B445**, 49 (1995).
- [15] H. Jung, M. Kraemer, A.V. Lipatov, and N.P. Zotov, Investigation of beauty production and parton shower effects at LHC, *Phys. Rev. D* **85**, 034035 (2012).
- [16] M. Aaboud *et al.* (ATLAS Collaboration), Measurement of b -hadron pair production with the ATLAS detector in proton-proton collisions at $\sqrt{s}=8$ TeV, [arXiv:1705.03374](https://arxiv.org/abs/1705.03374).
- [17] T. Sjostrand, S. Mrenna, and P.Z. Skands, A brief introduction to PYTHIA 8.1, *Comput. Phys. Commun.* **178**, 852 (2008).
- [18] T. Gleisberg, S. Hoeche, F. Krauss, M. Schonherr, S. Schumann, F. Siegert, and J. Winter, Event generation with SHERPA 1.1, *J. High Energy Phys.* **02** (2009) 007.
- [19] L.N. Lipatov, Gauge invariant effective action for high-energy processes in QCD, *Nucl. Phys.* **B452**, 369 (1995).
- [20] L.N. Lipatov and M.I. Vyazovsky, Quasi-multi-Regge processes with a quark exchange in the t channel, *Nucl. Phys.* **B597**, 399 (2001).
- [21] L.N. Lipatov, Small x physics in perturbative QCD, *Phys. Rep.* **286**, 131 (1997).
- [22] E.N. Antonov, L.N. Lipatov, E.A. Kuraev, and I.O. Cherednikov, Feynman rules for effective Regge action, *Nucl. Phys.* **B721**, 111 (2005).
- [23] J. Bartels, L.N. Lipatov, and G.P. Vacca, Ward Identities for Amplitudes with Reggeized gluons, *Phys. Rev. D* **86**, 105045 (2012).
- [24] J.R. Andersen, V. Del Duca, and C.D. White, Higgs Boson Production in Association with Multiple Hard Jets, *J. High Energy Phys.* **02** (2009) 015.
- [25] F. Hautmann, M. Hentschinski, and H. Jung, Forward Z-boson production and the unintegrated sea quark density, *Nucl. Phys.* **B865**, 54 (2012).
- [26] M. Nefedov and V. Saleev, Diphoton production at the Tevatron and the LHC in the NLO approximation of the parton Reggeization approach, *Phys. Rev. D* **92**, 094033 (2015).
- [27] A. Buckley *et al.*, General-purpose event generators for LHC physics, *Phys. Rep.* **504**, 145 (2011).
- [28] M.A. Kimber, A.D. Martin, and M.G. Ryskin, Unintegrated parton distributions, *Phys. Rev. D* **63**, 114027 (2001).
- [29] A.D. Martin, M.G. Ryskin, and G. Watt, NLO prescription for unintegrated parton distributions, *Eur. Phys. J. C* **66**, 163 (2010).
- [30] M.A. Nefedov, V.A. Saleev, and A.V. Shipilova, Dijet azimuthal decorrelations at the LHC in the parton Reggeization approach, *Phys. Rev. D* **87**, 094030 (2013).
- [31] V. Saleev and A. Shipilova, Inclusive b-jet and $b\bar{b}$ -dijet production at the LHC via Reggeized gluons, *Phys. Rev. D* **86**, 034032 (2012).
- [32] R. Maciula, V.A. Saleev, A.V. Shipilova, and A. Szczurek, New mechanisms for double charmed meson production at the LHCb, *Phys. Lett. B* **758**, 458 (2016).
- [33] A. Karpishkov, V. Saleev, and A. Shipilova, Large- p_T production of D mesons at the LHCb in the parton Reggeization approach, *Phys. Rev. D* **94**, 114012 (2016).
- [34] A.V. Karpishkov, M.A. Nefedov, V.A. Saleev, and A.V. Shipilova, B-meson production in the parton Reggeization approach at Tevatron and the LHC, *Int. J. Mod. Phys. A* **30**, 1550023 (2015).
- [35] B.A. Knieh, M.A. Nefedov, and V.A. Saleev, Prompt-photon plus jet associated photoproduction at HERA in the parton Reggeization approach, *Phys. Rev. D* **89**, 114016 (2014).
- [36] A. van Hameren and M. Serino, BCFW recursion for TMD parton scattering, *J. High Energy Phys.* **07** (2015) 010; K. Kutak, A. Hameren, and M. Serino, QCD amplitudes with 2 initial spacelike legs via generalised BCFW recursion, *J. High Energy Phys.* **02** (2017) 009.
- [37] A. van Hameren, KaTie: For parton-level event generation with k_T -dependent initial states, [arXiv:1611.00680](https://arxiv.org/abs/1611.00680).

- [38] A. D. Martin, W. J. Stirling, R. S. Thorne, and G. Watt, Parton distributions for the LHC, *Eur. Phys. J. C* **63**, 189 (2009).
- [39] B. A. Kniehl, G. Kramer, I. Schienbein, and H. Spiesberger, Finite-mass effects on inclusive B -meson hadroproduction, *Phys. Rev. D* **77**, 014011 (2008).
- [40] M. Cacciari, G. P. Salam, and G. Soyez, The anti- $k(t)$ jet clustering algorithm, *J. High Energy Phys.* **04** (2008) 063.
- [41] T. Hahn, Generating Feynman diagrams and amplitudes with FeynArts 3, *Comput. Phys. Commun.* **140**, 418 (2001).
- [42] T. Hahn and M. Perez-Victoria, Automatized one loop calculations in four-dimensions and D-dimensions, *Comput. Phys. Commun.* **118**, 153 (1999).
- [43] M. A. Nefedov and V. A. Saleev (to be published).
- [44] T. Hahn, CUBA: A library for multidimensional numerical integration, *Comput. Phys. Commun.* **168**, 78 (2005); Concurrent CUBA, *J. Phys. Conf. Ser.* **608**, 012066 (2015).
- [45] M. L. Mangano and J. Rojo, Cross Section Ratios between different CM energies at the LHC: Opportunities for precision measurements and BSM sensitivity, *J. High Energy Phys.* **08** (2012) 010.
- [46] D. Binosi and L. Theussl, JaxoDraw: A graphical user interface for drawing Feynman diagrams, *Comput. Phys. Commun.* **161**, 76 (2004).